

PCCP

Accepted Manuscript



This is an *Accepted Manuscript*, which has been through the Royal Society of Chemistry peer review process and has been accepted for publication.

Accepted Manuscripts are published online shortly after acceptance, before technical editing, formatting and proof reading. Using this free service, authors can make their results available to the community, in citable form, before we publish the edited article. We will replace this *Accepted Manuscript* with the edited and formatted *Advance Article* as soon as it is available.

You can find more information about *Accepted Manuscripts* in the [Information for Authors](#).

Please note that technical editing may introduce minor changes to the text and/or graphics, which may alter content. The journal's standard [Terms & Conditions](#) and the [Ethical guidelines](#) still apply. In no event shall the Royal Society of Chemistry be held responsible for any errors or omissions in this *Accepted Manuscript* or any consequences arising from the use of any information it contains.

Active Edge Sites in MoSe₂ and WSe₂ Catalysts for the Hydrogen Evolution Reaction: A Density Functional Study†

Charlie Tsai,^{ab} Karen Chan,^{ab} Frank Abild-Pedersen^b and Jens K. Nørskov^{*ab}

^a Department of Chemical Engineering, Stanford University, Stanford, California, 94305, USA

^b SUNCAT Center for Interface Science and Catalysis, SLAC National Accelerator Laboratory, 2575 Sand Hill Road, Menlo Park, California, 94025, USA

† Electronic supplementary information (ESI) available.

MoSe₂ and WSe₂ nanofilms and nanosheets have recently been shown to be active for electrochemical H₂ evolution (HER). In this work, we used periodic density functional theory to investigate the origin of the catalytic activity on these materials. We determined the relevant structures of the Mo/W-edges and the Se-edges under HER conditions and their differential hydrogen adsorption free energies. The Mo-edge on MoSe₂ and the Se-edge on both MoSe₂ and WSe₂ are found to be the predominantly active facets for these catalysts, with activity predicted to be comparable to or better than MoS₂. On the other hand, the (0001) basal planes are found to be inert. We further explain the enhanced activity at the edges in terms of localized edge states, which provide insight into the trends in HER activity seen between the two catalysts. Our results thus suggest that an optimal catalyst design should maximize the exposure of edge sites. Comparisons are made between the transition metal selenide catalysts and their sulfide counterparts in order to understand the consequences of having either Mo/W or Se/S atoms. It is found that linear scaling relations describe the S/Se binding onto the edge and the H binding onto the S/Se.

Introduction

The electrochemical hydrogen evolution reaction (HER) has been suggested as a possible route to the sustainable production of H₂.¹ As the expensive and scarce Pt group metals^{2,3} are currently the most effective at catalyzing this reaction, alternative catalysts that are cheap and based on earth-abundant elements are needed for large scale production. HER involves hydrogen binding to the catalyst surface in the first step, and the hydrogen adsorption free energy has been shown to be a good descriptor for the rate of reaction, with an optimal binding energy of $\Delta G_{\text{H}} \approx 0$ eV.²⁻⁶

Layered transition metal dichalcogenides (TMD) have been gaining widespread attention for the design of novel materials due to their unique chemical and physical properties. It is now well known that layered TMD's can be exfoliated into two-dimensional sheets,⁷⁻¹² similar to graphene. A well known example for HER is MoS₂, which was first predicted by theory¹³ and then experimentally proven in a number of studies to have better activity than most non-precious metals.¹³⁻²² It has been shown that the edge states at the MoS₂ edges are responsible for this enhanced activity, while the basal plane is inert and insulating.²³⁻²⁶ Similar experimental HER studies have been done on other TMD's, including WS₂, MoSe₂, and WSe₂,^{18,22,27-29} all of which demonstrate promising activity for HER. However, a comprehensive theoretical study of the structure and activity of MoSe₂ and WSe₂ catalysts is currently lacking. At the moment, it is unknown whether it is the basal plane, the Mo/W-edge, or the Se-edge that is responsible for the catalytic activity in each of these catalysts. Furthermore, the exact edge structures involved under reaction conditions have not yet been determined. A wide range of adsorption structures are possible depending on the edge coverage of Se assumed, so it is crucial to determine the relevant configuration in order to obtain an accurate theoretical prediction of activity for these materials.

In this work, we use density functional theory (DFT) to investigate the edge and basal plane sites of MoSe₂ and WSe₂ for the hydrogen evolution reaction. We first determine the relevant Se configurations of the (10 $\bar{1}$ 0) Mo/W-edge and the ($\bar{1}$ 010) Se-edge under HER conditions. Then, we use the ΔG_{H} to compare the relative HER activity between the basal plane and edges. Our results confirm that the edge sites of MoSe₂ and WSe₂ should be the active centers for HER, with comparable or possibly higher activity than MoS₂. We find the enhanced activity at the edges to arise from the one-dimensional edge states, in further analogy to MoS₂.^{2,3,24} In order to understand the consequences of changing either the transition metal (Mo or W) or chalcogen (Se or S) in the layered structure, we have calculated the chalcogen, X, and HX binding energy onto the stable edge, where X = Se or S. We find an anti-correlation between X binding and H binding that indicates that hydrogen adsorption is directly mediated by how strongly the chalcogen is bound to the transition metal.

Methods

Setup and calculation details

Plane-wave DFT employing ultrasoft-pseudopotentials was used to calculate the structures and electronic energies. The QUANTUM ESPRESSO code^{2-6,30} and the BEEF-vdW exchange-correlation functional^{7-12,31-34} were used for all calculations. The plane-wave cutoff and density cutoff were 500 eV and 5000 eV respectively. The bulk lattice constants (experimental values in parentheses) were determined to be $a = 3.35 \text{ \AA}$ (3.288 \AA), $c = 13.78 \text{ \AA}$ (12.900 \AA) for MoSe₂ and $a = 3.33 \text{ \AA}$ (3.280 \AA), $c = 14.06 \text{ \AA}$ (12.950 \AA) for WSe₂, in reasonable agreement with experimentally measured values.³⁵ An infinite stripe model described previously^{13-22,24,25} was used to investigate the (10 $\bar{1}$ 0) Mo/W-edge and ($\bar{1}$ 010) Se-edge, whereas an infinite slab was used to model the (0001) basal plane (Fig. 1.).

The coverage of hydrogen is defined as the fraction of a monolayer with respect to the number of available Se atoms on either the edge or the basal plane,

$$\theta_{\text{H}} (\text{ML}) = n_{\text{H}}/(\text{Se atoms}) \quad (1)$$

We define the coverage of selenide atoms at the edge as

$$\theta_{\text{Se}} (\text{ML}) = n_{\text{Se}}/(2 \times \text{edge length}) \quad (2)$$

The differential hydrogen adsorption free energies (ΔG_{H}) were defined in the same way as described previously.^{23-26,36} For example, ΔG_{H} at $\theta_{\text{H}} = 0.25 \text{ ML}$ refers to the adsorption free energy for increasing the hydrogen coverage from 0 ML to 0.25 ML, whereas a ΔG_{H} at $\theta_{\text{H}} = 0.5 \text{ ML}$ refers to the adsorption free energy for increasing the hydrogen coverage from 0.25 ML to 0.5 ML.

Two unit cell sizes were used to describe both the basal plane and the edges (represented as solid and dotted lines respectively in Figure 1). The first unit cell was two Mo/W wide in the x -direction and four Mo/W wide in the y -direction, which allows us to describe hydrogen coverages at the edge of $\theta_{\text{H}} = 0 \text{ ML}$, 0.5 ML and 1.0 ML . The second unit cell was four Mo/W wide in the x -direction and four Mo/W wide in the y -direction, which allows us to describe hydrogen coverages at the edge of $\theta_{\text{H}} = 0.25 \text{ ML}$ and 0.75 ML . For Se coverages at the edge greater than $\theta_{\text{Se}} = 0.5 \text{ ML}$, the larger unit cell was used to account for possible edge reconstruction along the x -direction. To verify that the two edges are sufficiently decoupled in the y -direction, all atoms were allowed to relax. It was found that four Mo/W atoms in the y -direction were sufficient to prevent any changes in one edge from affecting the other. In all cases, periodic boundary conditions were used along with 11 \AA of vacuum in the z -direction to separate neighboring slabs and 9 \AA of vacuum in the y -direction to separate the infinite stripes. The Brillouin zone was sampled by a Monkhorst-Pack $4 \times 1 \times 1$ k -point grid for the first unit cell and $2 \times 1 \times 1$ k -point grid for the second unit cell^{18,22,27,28,37} and structures were relaxed until the total force were less than 0.05 eV/\AA.

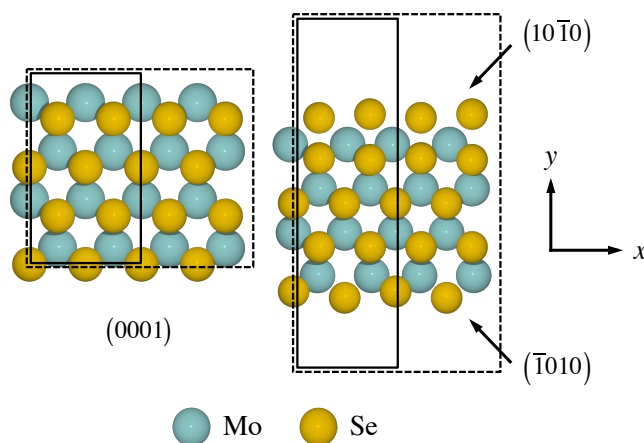


Figure 1. Calculation unit cells. Shown for MoSe_2 . Left: infinite slab used to model the basal plane. Right: infinite stripe used to model the edge sites. The smaller unit cell (solid lines) and larger unit cell (dotted line) are both shown. The $(10\bar{1}0)$ Mo-edge and $(\bar{1}010)$ Se-edge both terminate with Se atoms.

Edge structure determination

It is crucial to have the correct edge structure for the reaction conditions, as the ΔG_{H} can change drastically depending on the coverage of Se at the edge. The ΔG_{H} for the Se-edge of MoSe_2 for instance varies from -0.4 eV to 0.5 eV for $\theta_{\text{Se}} = 0$ ML to 1.0 ML. The edge free energy^{25,38} is given by,

$$\gamma = \frac{1}{2L} \left[G(M\text{Se}_2 + N_{\text{H}}\text{H}) - N_{\text{M}}E_{M\text{Se}_2}^{\text{bulk}} + (2N_{\text{M}} - N_{\text{Se}})\mu_{\text{Se}} - N_{\text{H}}\mu_{\text{H}} \right] \quad (3)$$

where L is the length of the edge in the unit cell, N_i is the number of atoms of $i = \text{H}$ or M , where $M = \text{Mo}$ or W , $E_{M\text{Se}_2}^{\text{bulk}}$ is the bulk energy of $M\text{Se}_2$, and μ_{H} and μ_{Se} are the chemical potentials for H and Se. The following equilibrium reactions determine the chemical potentials:



and



where $(*)$ denotes a selenide vacancy on the edge. Using the computational hydrogen electrode^{5,39} (CHE), the chemical potentials are,

$$\mu_{\text{Se}} = \mu_{\text{H}_2\text{Se}} - 2 \left(\frac{1}{2} \mu_{\text{H}_2} - eU_{\text{RHE}} \right) \quad (6)$$

$$\mu_{\text{H}} = \frac{1}{2} \mu_{\text{H}_2} - eU_{\text{RHE}} \quad (7)$$

where U_{RHE} is the potential versus the reversible hydrogen electrode. Due to the negligible pressure of H_2Se under reaction conditions, the chemical potential for Se is expected to be extremely negative and a simple minimization of the edge free energy γ would imply that the Se atoms at the edge should dissolve completely according to reaction 4. However, at reducing potentials of $U_{\text{RHE}} < 0 \text{ V}_{\text{RHE}}$, the relevant coverage is determined by kinetics, where hydrogen evolution on the Se (reaction 5) competes with the vacancy formation from Se desorption as

H₂Se (reaction 4). To determine the relevant edge configuration under HER conditions, we first start with the thermodynamically stable edge coverage at 0 V_{RHE}, and a H₂Se pressure of 10⁻⁵ and 10⁻⁸ bar corresponding to a standard corrosion resistance.⁴⁰ The potential was assumed to be $U = 0$ V_{RHE} as a starting point because we are interested in the region of low overpotential. We then assume that the relevant coverage corresponds to when HER is further downhill than H₂Se desorption or further H adsorption. An example of edge structure determination on the Mo-edge of MoSe₂ is shown in Figure 2, where the edge free energies γ are plotted. Figure 3 shows the free energy diagrams confirming that H₂ evolution is the most downhill reaction on these structures. A For both the (10 $\bar{1}$ 0) edges and ($\bar{1}$ 010) edges, we considered Se coverages of $\theta_{\text{Se}} = 0, 0.25, 0.5, 0.75,$ and 1.0 ML (details of the structures considered are in the supporting information).

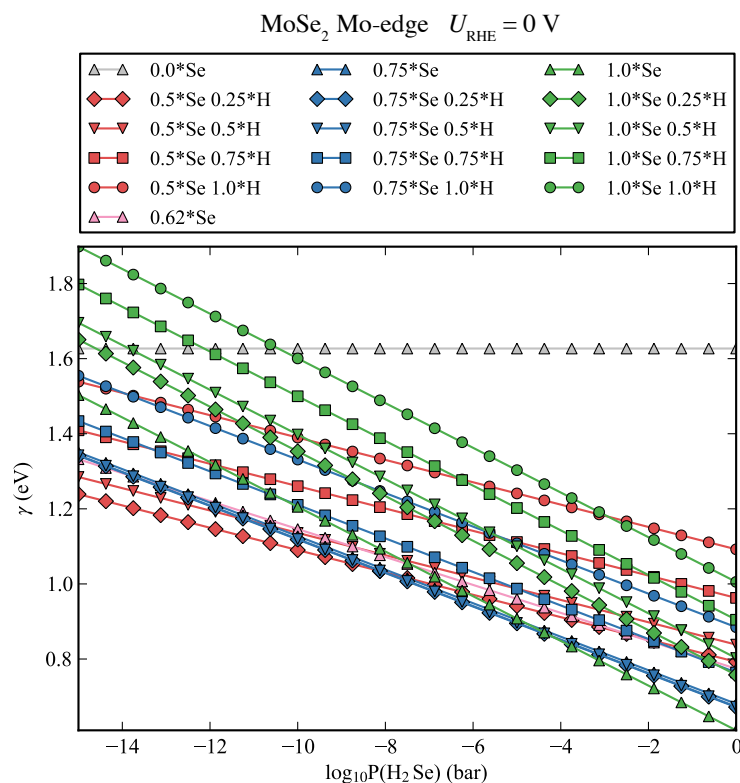


Figure 2. Example of the edge free energy γ as a function of H₂Se pressure for each configuration of Se on the Mo-edge on MoSe₂. Each edge free energy line corresponds to a possible edge structure. The most thermodynamically stable coverage was found to be 0.5 ML Se or 0.75 ML from the plot in the range of 10⁻⁵ to 10⁻⁸ bar of H₂Se.

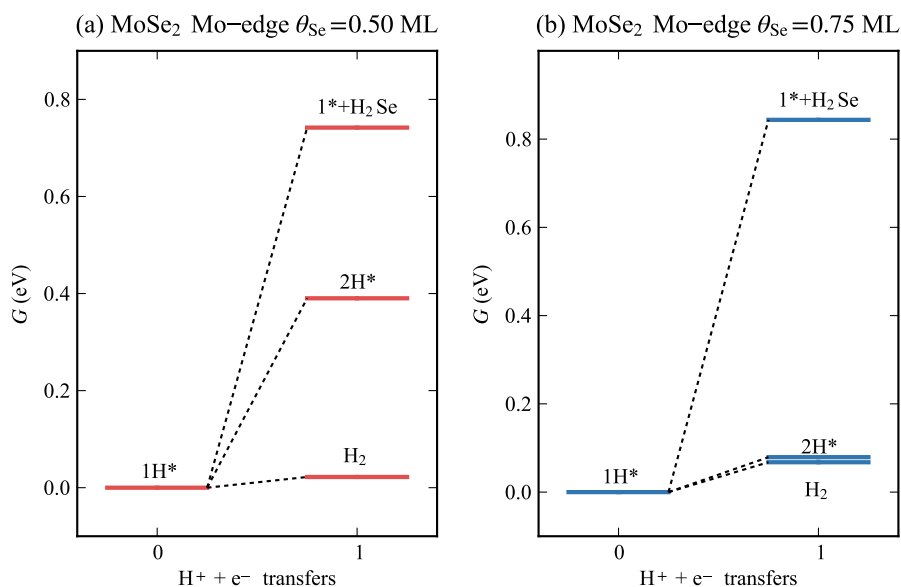
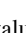
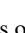

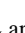


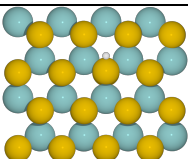
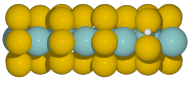
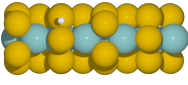
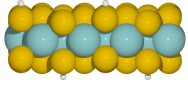
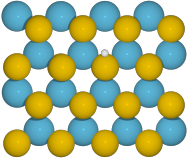
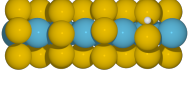
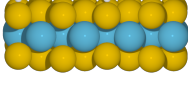
Figure 3. Example free energy diagrams for the Mo-edge of MoSe₂ that confirm that (a) 0.5 ML Se with 0.25 ML H and (b) 0.75 ML Se with 0.25 ML H are the relevant coverage for HER. Further H₂Se desorption or H adsorptions are more uphill in energy compared to H₂ evolution. H* denotes an adsorbed hydrogen and * denotes a selenide vacancy site. Details for all the edge structures considered are in the supporting information.

Comparison with MoS₂ and WS₂

In order to directly compare MoSe₂ and WSe₂ to their sulfide counterparts, we recalculated the previously published results on MoS₂^{13,25} and WS₂¹⁸ using the BEEF-vdW exchange-correlation functional (previous calculations used the RPBE exchange-correlation functional⁴¹). The new bulk lattice parameters (with experimental values in parentheses) were determined to be $a = 3.19$ Å (3.20 Å), $c = 13.05$ Å (12.29 Å) for MoS₂ and $a = 3.20$ Å (3.162 Å)⁴², $c = 13.33$ Å (12.35 Å)⁴³ for WS₂. Theoretical and experimental values are in reasonable agreement. The same detailed analysis for determining the stable edge structures was also performed on MoS₂ and WS₂. It was found that for the Mo-edge and W-edge, the coverage of sulfur atoms was 0.5 ML whereas for the S-edges, the coverages were 1.0 ML. The results are summarized in Table 2.

Results and discussion

Table 1. The structures and hydrogen adsorption free energies for MoSe₂ and WSe₂. Only the most stable edge configurations are shown. All values of ΔG_{H} are shown for the final adsorbed hydrogen at the corresponding θ_{H} . (Mo = , W = , Se = , H = )

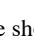
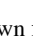
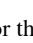
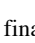
System	Surface	Stable Structure	θ_{Se} (ML)	θ_{H} (ML)	H adsorption ΔG_{H} (eV)
MoSe ₂					
	Basal plane (0001)			0.0625	2.13
	Mo-edge (10 $\bar{1}$ 0)		0.5	0.25	0.02
	Mo-edge (10 $\bar{1}$ 0)		0.75	0.25	-0.04
	Se-edge ($\bar{1}$ 010)		1.0	1.0	-0.05
WSe ₂					
	Basal plane (0001)			0.0625	2.31
	W-edge (10 $\bar{1}$ 0)		0.5	0.25	0.17
	Se-edge ($\bar{1}$ 010)		1.0	0.50	-0.05

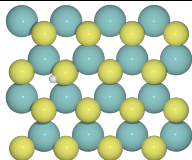
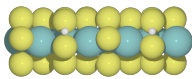
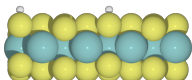
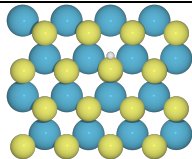
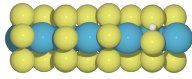
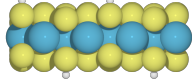
Differential hydrogen adsorption free energies on MoSe₂ and WSe₂

Table 1 shows the structures, hydrogen coverages, and ΔG_{H} of the (0001) basal plane, (10 $\bar{1}$ 0) edge, and ($\bar{1}$ 010) edge. The differential hydrogen adsorption free energy, ΔG_{H} , is shown for the final hydrogen added on at the coverage, θ_{H} , shown. For both the basal plane and the edges, this coverage θ_{H} represents the maximum hydrogen coverage beyond which no further hydrogen could be adsorbed (i.e. it is easier to remove hydrogen than to absorb additional hydrogen at this coverage). All adsorbates are considered at the lowest energy binding sites. The ΔG_{H} on the basal planes are approximately 2 eV for both MoSe₂ and WSe₂, which indicate that the basal plane is inert. For the edge structures, the H atoms were found to preferentially bind on every other Se site rather than to the neighboring Se atom, in analogy with MoS₂ (also shown in Table 1).¹³ More involved kinetic barriers will have to be calculated to determine the specific mechanism for HER; regardless, the differential hydrogen adsorption free energy on the structurally similar MoS₂ was found to describe the HER activity well, so we also assume that to be the case here.^{15,44}

For the Mo-edge of MoSe₂, it was determined that Se coverages of 0.5 ML and 0.75 ML are very close in edge energy and could both be stable (Figure 2). Without accurate kinetic barriers for defect formation, it is not possible to clearly distinguish between the two. The hydrogen adsorption free energies are similarly close to

thermoneutral ($\Delta G_{\text{H}} = 0.02$ eV and $\Delta G_{\text{H}} = -0.04$ eV, respectively) and both predicted to be active for HER. The Se-edge of MoSe_2 was determined to have similar hydrogen binding as the Mo-edge ($\Delta G_{\text{H}} = -0.05$ eV). The two edges of MoSe_2 are thus expected to be approximately equal in HER activity. For WSe_2 , the W-edge has a hydrogen adsorption free energy of $\Delta G_{\text{H}} = 0.17$ eV while at the Se-edge it is -0.05 eV. According to a previously determined activity map for HER, this difference in ΔG_{H} represents about an order of magnitude difference in the turnover rate.⁴⁵ The Se-edge of WSe_2 is thus expected to be the primary active site for HER. We find that our results qualitatively agree with the experimental studies done on vertically standing MoSe_2 and WSe_2 nanofilms.^{22,27} In these model systems, only the edge sites are exposed and the two edges are expected to be present in approximately equal amounts. For both types of edges, MoSe_2 has the most thermoneutral ΔG_{H} compared to WSe_2 , so it should be the more active catalyst, which is consistent with the experimental trends from Wang et. al.²⁷

Table 2. For comparison, the structures and hydrogen adsorption free energies for MoS_2 and WS_2 . Only the most stable edge configurations are shown. All values of ΔG_{H} are shown for the final adsorbed hydrogen at the corresponding θ_{H} . (Mo = , W = , S = , H = )

System	Surface	Stable Structure	θ_{S} (ML)	θ_{H} (ML)	H adsorption ΔG_{H} (eV)
MoS₂					
	Basal plane (0001)			0.0625	1.92
	Mo-edge (10 $\bar{1}$ 0)		0.5	0.25	0.06
	S-edge ($\bar{1}$ 010)		1.0	1.0	-0.45
WS₂					
	Basal plane (0001)			0.0625	2.23
	W-edge (10 $\bar{1}$ 0)		0.5	0.25	-0.04
	S-edge ($\bar{1}$ 010)		1.0	1.0	-0.06

Comparing the Edge Structure and Adsorption Energies with MoS_2 and WS_2

Table 2 shows the structures, hydrogen coverages, and hydrogen adsorption free energies for MoS_2 and WS_2 . The edge structures have been determined in the same way as the selenides, which is a more thorough analysis of the thermodynamics involved under electrochemical conditions compared to previous studies on MoS_2 and WS_2 .^{13,18} In terms of hydrogen adsorption free energies, the basal planes of MoSe_2 , WSe_2 , MoS_2 , and WS_2 are almost identically inert with $\Delta G_{\text{H}} \approx 2$ eV (Table 1 and Table 2). This suggests that the inertness of the basal plane

of group 6 layered TMD's is relatively insensitive to the choice of transition metal (Mo or W) or chalcogen (Se or S). The two edges on MoSe₂ and the Se-edge of WSe₂ have comparable HER activity to the MoS₂ Mo-edge and the two edges of WS₂, which have $|\Delta G_{\text{H}}|$ of approximately 0.05 eV (Table 2). Among the four, MoSe₂ is predicted to be the most active catalyst, followed closely by WS₂, as they have the most thermoneutral ΔG_{H} for both edges.

It is worth noting that all edges have ΔG_{H} similarly close to 0 eV except for the W-edge of WSe₂ or the S-edge of MoS₂. The W-edge of WSe₂ binds hydrogen weakly so HER will be comparatively more difficult even at the lowest possible hydrogen coverage. The S-edge of MoS₂ on the other hand, binds hydrogen too strongly, leading to hydrogen being poisoned at the sites even at the highest possible coverage. All other edge structures have more intermediate binding of hydrogen, so as long as they have a saturated coverage of hydrogen within the constraints of our unit cell size, the ΔG_{H} is relatively close to thermoneutral.

To understand the consequences of having each combination of transition metal (Mo or W) and chalcogen (Se or S), we calculated the HX adsorption energy (where $X = \text{S, Se}$) at the edge, ΔE_{HX} , which is defined as

$$\Delta E_{\text{HX}} = E(\text{MX}_2) + \frac{1}{2}E(\text{H}_2) - E(\text{MX}_2 - \text{HX}) - E(\text{H}_2\text{X}) \quad (8)$$

where $M = \text{Mo, W}$, and $X = \text{S, Se}$, and HX is adsorbed onto a vacancy from the stable edge structures shown in Table 1 and Table 2 (i.e. the negative of the HX removal energy from the stable edge structures). The adsorption energy of $X = \text{S or Se}$ (ΔE_X) was calculated as the negative of the energy for the removal of S or Se in the edge structure relative to bulk S or Se.

We show ΔE_{HX} as a function of ΔE_X in Figure 4, where a positive linear scaling relationship exists, indicating that the strength of X adsorption onto the edge is directly related to how stable the edge is (how difficult it would be to remove HX as H₂X). Regardless, when hydrogen adsorption free energy (ΔG_{H}) is shown as a function of ΔE_X , we find a negative scaling relationship between how strongly X is bound and how strongly H is bound onto X. This suggests that the strength of X binding to the edge determines the binding strength of H. X that is bound more strongly onto the edge leads to H that is bound more weakly to X.

The consequence of changing the transition metal (Mo or W), or the edge type (Mo/W-edge or S/Se-edge), is then simply to shift along these scaling lines. W containing edges tend to bind X more strongly than their Mo counterparts, and hence have weaker hydrogen binding for the same type of edge. For all edge types, the HSe group tends to be bound more strongly than the HS group, resulting in weaker hydrogen binding for Se containing edges. This is reflected in the downshifted ΔE_X vs. ΔE_{HX} scaling line and the upshifted ΔE_X vs. ΔG_{H} scaling line. In general there is at least a small amount of edge structure reorganization upon H adsorption, which could explain some of the spread in the data in Figure 4.

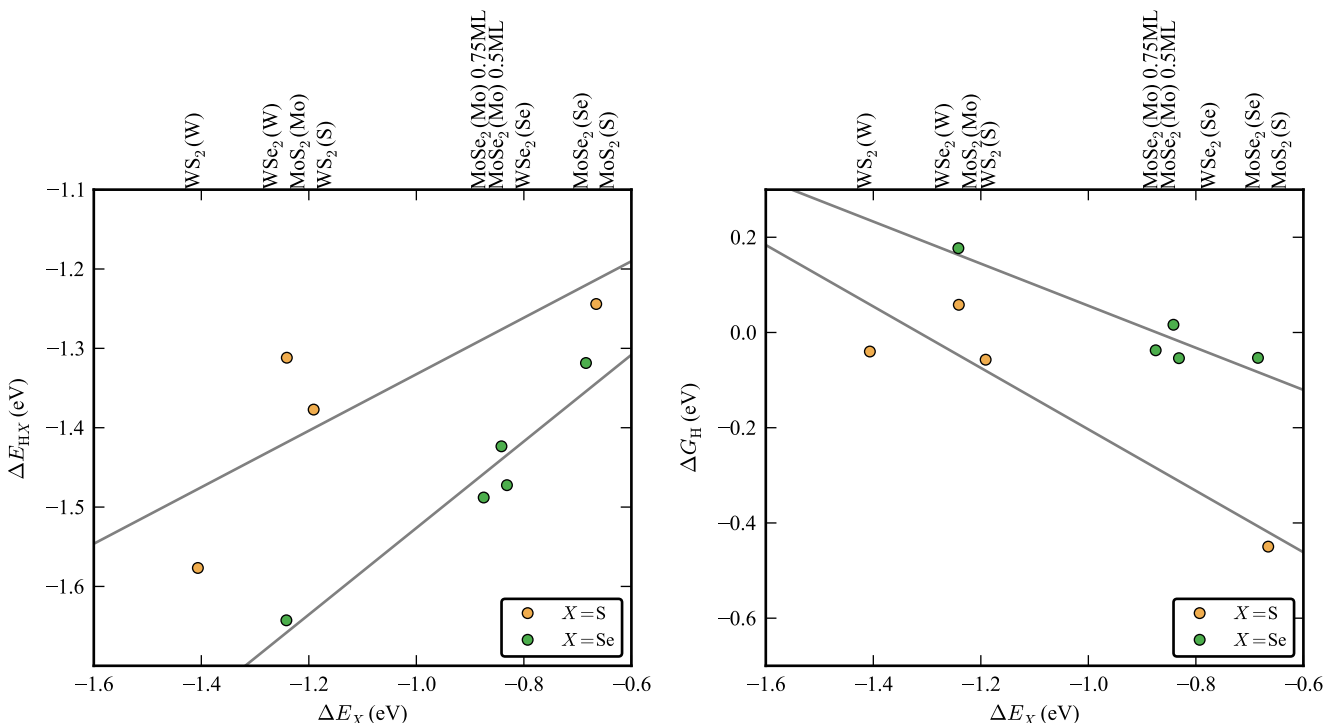


Figure 4. Plot of HX adsorption energy and hydrogen adsorption free energy (ΔG_{H}) as a function of X adsorption energy (ΔE_X) where $X = \text{S}, \text{Se}$. The strength of X binding indicates how strongly the entire HX group is bound to the edge, while X binding is also negatively correlated with how strongly H is bound onto X . There is then a compensation effect between how strongly X is bound onto the metal and how strongly H is bound onto X .

Relating the electronic structure of the edge to the catalytic activity

Since the chemical properties of the edge sites are defined by the underlying electronic structure, an analysis of the density of states at the edges can give us additional insight into the trends in the hydrogen adsorption free energies. The selenide atoms interact directly with hydrogen, so we focus on the p -density of states here. Figure 5 shows the atom-projected p -orbital density of states of the Se atoms and the s -orbital density of states of the adsorbed H atoms. These were calculated from the structures given in Table 1 with one H removed. These are organized from top to bottom in order of decreasing H adsorption free energy. Since H binds directly to the Se atoms at the edge, the Se states should give a direct means of studying the hydrogen binding.

There is significant reconstruction at the Se-edge of WSe_2 upon H adsorption, so the ΔG_{H} listed in Table 1 will include this contribution. The bond in the Se–Se dimer is broken in order to form the Se–H bond (see supporting information Table S4.), which increases the Se–Se bond distance from 2.39 Å to 3.03 Å. Subtracting the energetic cost for this reconstruction (0.10 eV) from the ΔG_{H} results in a Se–H bond formation free energy of -0.15 eV, which is the value shown in Figure 5.

From the p -projected density of states on the Se atoms, we see sharp resonant states at the Fermi level for all the considered edges (Figure 5a). In analogy with MoS_2 , the presence of localized edge states is responsible for the enhanced binding relative to the basal plane.^{24,25} When the s -states of the hydrogen adsorbate (the adsorbate state, shown in Figure 5a) interact with the resonant p -states of Se on the edge, it gives rise to bonding and anti-bonding states,^{46,47} shown in Figure 5b. Despite the visible shift in the p -states, there does not appear to be a change in the filling of either the bonding or the anti-bonding s -states, so the shifting of the s -states cannot explain the trends in H binding. Instead, if one assumes that the partially filled resonant p -states and the adsorbate state can be approximated by single energy levels ϵ_p and ϵ_s , respectively, then one can look at the interaction energy in the perturbation limit for a qualitative explanation of the trends,^{46,48}

$$\Delta\epsilon \sim -\frac{V^2}{|\epsilon_p - \epsilon_s|} \quad (9)$$

where $\Delta\varepsilon$ is the interaction energy, “ \sim ” represents proportionality, and V is the coupling matrix element. For the position of the renormalized adsorbate state, we assume a fixed value of $\varepsilon_s = 0$ eV relative to the Fermi level. The exact position of ε_s is unimportant for such a qualitative analysis. Assuming that V is constant across the edge structures, the variation in H adsorption is then determined by the denominator, $|\varepsilon_p - \varepsilon_s|$, in Equation 9. The attractive interaction will be strongest when $|\varepsilon_p - \varepsilon_s|$ is minimized. From Figure 5a, we see that the trends in ΔG_H follow this conclusion exactly: the edge structures with ε_p and ε_s closest together have the most negative H adsorption free energies, whereas edge structures with ε_p and ε_s furthest apart have the most positive H adsorption free energies. It should be noted that even though the shift in the p -states describes the ΔG_H trends well, it becomes more complicated in cases such as the Se-edge of WSe_2 where significant edge reconstruction takes place, as the energetic contribution of the reconstruction is not captured by the position of the p -states.

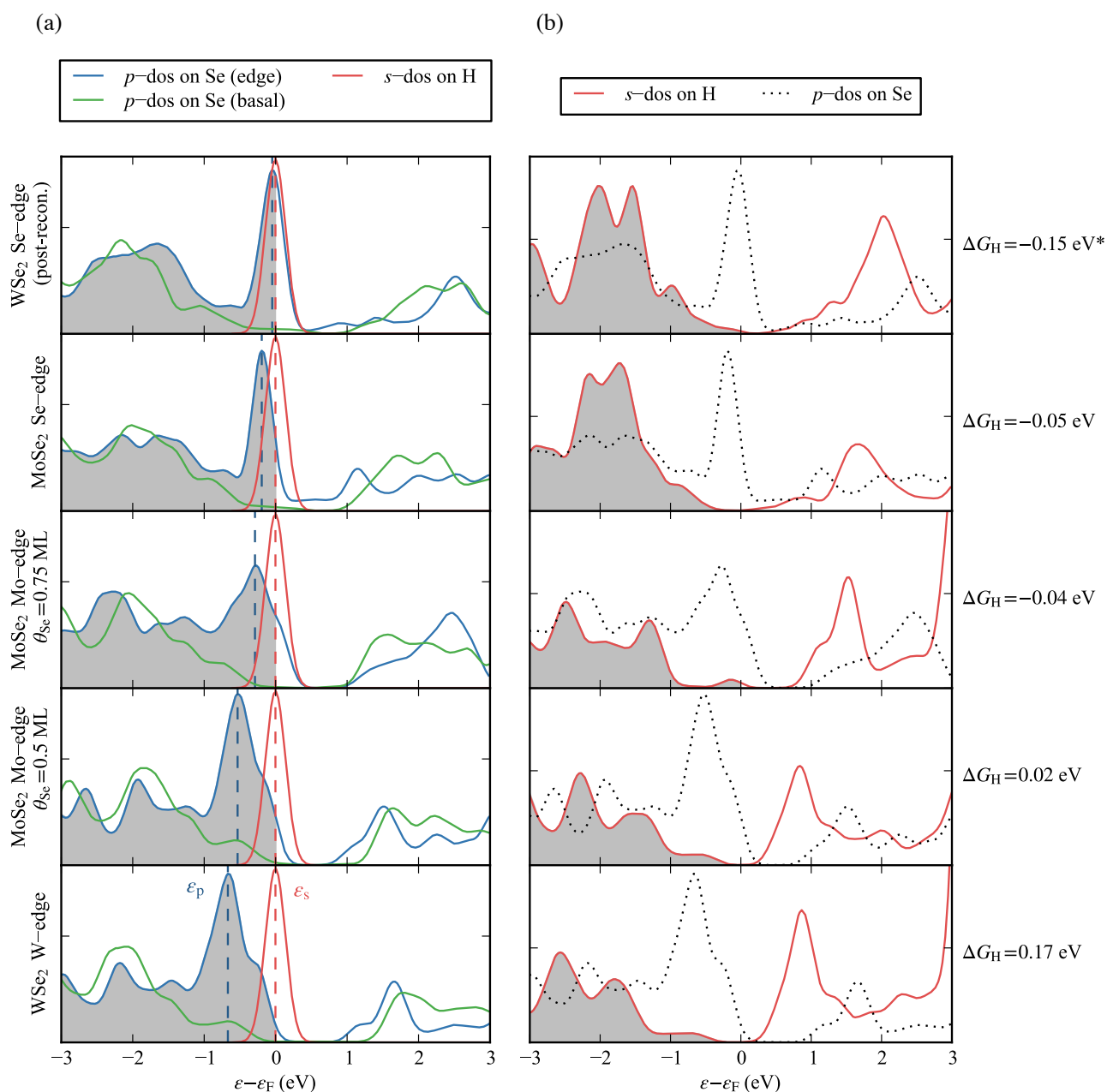


Figure 5. Projected density of states (PDOS) in arbitrary units, sorted by increasing ΔG_{H} from top to bottom. (a) p -density of states relative to the Fermi level projected onto Se atoms in MoSe_2 and WSe_2 . The blue lines indicate Se atoms on the edge, whereas the green lines indicate Se atoms in the basal plane. The red lines indicate the adsorbate state for the H. The shaded area indicates the states filled up to the Fermi level, ε_{F} . The dashed lines indicate the single energy levels ε_{p} and ε_{s} for the p -states and the adsorbate state, respectively. The densities of states were calculated at the coverages shown in Table 1 with the final adsorbed hydrogen removed. *There is significant reconstruction on the Se-edge of WSe_2 upon H adsorption, so the PDOS was calculated for the reconstructed structure with the H removed. The ΔG_{H} here has the energetic cost for reconstruction removed. (b) s -density of states projected onto adsorbed H showing the bonding and anti-bonding states relative to the Fermi level ε_{F} . In all cases, the filling of the bonding and anti-bonding states is unchanged despite the visible shift in the p -states (shown alongside for comparison). The densities of states were calculated at the coverages shown in Table 1.

To understand the role of the electronic structure of metal atoms at the edge (Mo or W), we have calculated the d -projected density of states onto the metal atom (Figure 6). These were calculated at the edges with $\theta_{\text{Se}} = 0$ ML. The trends in the d -band centers relative to the Fermi level, ε_{d} , are seen to correlate with the Se adsorption energies, ΔE_{Se} , onto the stable edge structures shown in Table 1 and 2. The densities of states in Figure 6 are ordered from top to bottom in decreasing ΔE_{Se} (increasing Se binding strength). A further upshifted d -band center relative to the Fermi level corresponds to stronger Se binding, and a more downshifted d -band center to weaker Se binding. The edges with approximately equal Se binding have d -band centers in the same position. Due to the anti-correlation between Se binding and H binding, the d -states then indirectly indicate the H binding strength through the correlation with Se binding.

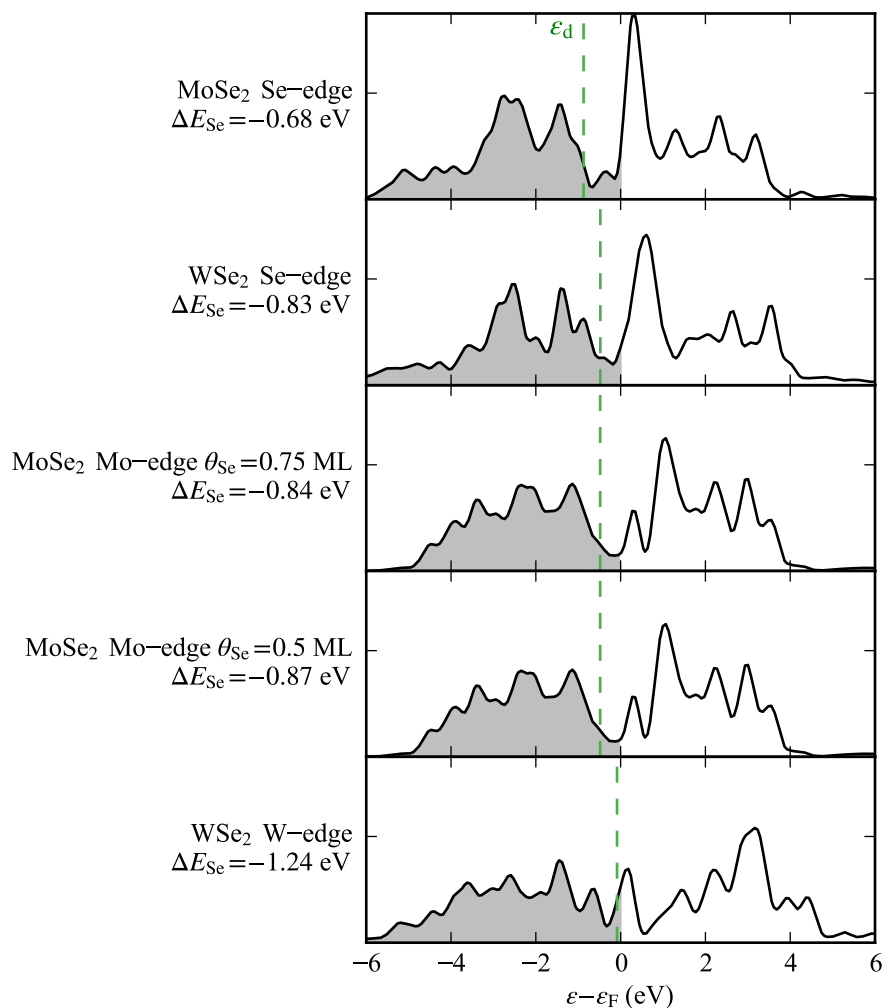


Figure 6. Projected d -density of states in arbitrary units, sorted by decreasing Se binding energy, ΔE_{Se} , from top to bottom. The edges with stronger Se binding exhibit larger upshifts in the d -states toward the Fermi level. The green dashed line indicates the d -band center, ε_{d} . The shaded area indicates the states filled up to the Fermi level, ε_{F} .

Conclusions

In this study, we have used DFT to investigate the atomic and electronic structure of MoSe₂ and WSe₂ for the hydrogen evolution reaction. We determined the relevant edge configurations for the reaction conditions and found the Mo-edge of MoSe₂ and the Se-edges of both MoSe₂ and WSe₂ to be the major sites for catalytic activity. The enhanced activity on the edges compared to the inert basal planes arises from the localized edge states, whose positions relative to the Fermi level are consistent with the relative activity between the edges. Similar to MoS₂, an optimal design for MoSe₂ and WSe₂ nanocatalysts would therefore maximize the exposure of edge sites. While we have shown previously that the support could play a role in modifying the edge activity of MoS₂,⁴⁴ more work is being done to investigate the general trends in support interactions in other layered TMD's. We have also made comparisons with MoS₂ and WS₂, where we found that the edge structures were similar and the basal planes were almost identically inert. For both Se and S containing layered TMD's, linear negative scaling relationships were found to describe the chalcogen (Se or S) binding on the edge and H binding onto the chalcogen. In MoSe₂ and WSe₂, the HSe group tended to bind more strongly and H was correspondingly bound more weakly onto Se. Although we have only looked at a few layered transition metal selenides and sulfides, this compensation effect could be a general feature of the edge sites of layered TMD's. This suggests that the metal atom at the edge could be modified by dopant substitution to tune the hydrogen binding energy, which could be crucial for electrochemical reactions where HER is an undesirable competing reaction.

Using hydrogen binding as a simple probe for chemical activity, we show that the edge sites of MoSe₂ and WSe₂ may be of interest for a broader set of reactions. Having the relevant edge structures enables a proper theoretical investigation of these materials for other electrochemical processes where HER is an important competing reaction. Similarities between MoSe₂ and WSe₂ and their sulfide counterparts also suggest that the presence of active edge sites may be a general feature of layered TMD's. This opens up the possibility of studying the layered TMD's as a general class of catalysts. These possibilities will be examined in further studies.

Acknowledgments

We acknowledge support from the Center on Nanostructuring for Efficient Energy Conversion (CNEEC) at Stanford University, an Energy Frontier Research Center funded by the U.S. Department of Energy, Office of Basic Energy Sciences under award number DE-SC0001060. C.T. acknowledges support from the National Science Foundation Graduate Research Fellowship Program (GRFP) Grant DGE-114747. K.C. acknowledges support from the Air Force Office of Scientific Research through the MURI program under AFOSR Award No. FA9550-10-1-0572.

References

1. M. S. Dresselhaus and I. L. Thomas, *Nature*, 2001, **414**, 332–337.
2. R. Parsons, *Trans. Faraday Soc.*, 1958, **54**, 1053–1063.
3. S. Trasatti, *J. Electroanal. Chem.*, 1971, **33**, 351–378.
4. S. Trasatti, in *Advances in Electrochemical Science and Engineering, Volume 2*, eds. H. Gerischer and C. W. Tobias, Wiley.
5. J. K. Nørskov, T. Bligaard, Á. Logadóttir, J. R. Kitchin, J. G. Chen, S. Pandelov, and U. Stimming, *J. Electrochem. Soc.*, 2005, **152**, J23–J26.
6. J. Greeley, T. F. Jaramillo, J. L. Bonde, I. Chorkendorff, and J. K. Nørskov, *Nat. Mater.*, 2006, **5**, 909–913.
7. M. B. Dines, *Mater. Res. Bull.*, 1975, **10**, 287–291.
8. D. W. Murphy, *J. Chem. Phys.*, 1975, **62**, 973–978.
9. C. Liu, O. Singh, P. Joensen, A. E. Curzon, and R. F. Frindt, *Thin Solid Films*, 1984, **113**, 165–172.
10. P. Joensen, R. F. Frindt, and S. R. Morrison, *Mater. Res. Bull.*, 1986, **21**, 457–461.
11. D. Yang and R. F. Frindt, *J. Phys. Chem. Solids*, 1996, **57**, 1113–1116.
12. R. A. Gordon, D. Yang, E. D. Crozier, D. T. Jiang, and R. F. Frindt, *Phys. Rev. B*, 2002, **65**, 125407.
13. B. Hinnemann, P. G. Moses, J. L. Bonde, K. P. Jørgensen, J. H. Nielsen, S. Horch, I. Chorkendorff, and J. K. Nørskov, *J. Am. Chem. Soc.*, 2005, **127**, 5308–5309.
14. L. S. Byskov, J. K. Nørskov, B. S. Clausen, and H. Topsøe, *J. Catal.*, 1999, **187**, 109–122.

15. T. F. Jaramillo, K. P. Jørgensen, J. L. Bonde, J. H. Nielsen, S. Horch, and I. Chorkendorff, *Science*, 2007, **317**, 100–102.
16. Y. Li, H. Wang, L. Xie, Y. Liang, G. Hong, and H. Dai, *J. Am. Chem. Soc.*, 2011, **133**, 7296–7299.
17. J. Kibsgaard, Z. Chen, B. N. Reinecke, and T. F. Jaramillo, *Nat. Mater.*, 2012, **11**, 963–969.
18. J. L. Bonde, P. G. Moses, T. F. Jaramillo, J. K. Nørskov, and I. Chorkendorff, *Faraday Discuss.*, 2008, **140**, 219.
19. A. B. Laursen, S. Kegnæs, S. Dahl, and I. Chorkendorff, *Energy Environ. Sci.*, 2012, **5**, 5577–5591.
20. Z. Chen, A. J. Forman, and T. F. Jaramillo, *J. Phys. Chem. C*, 2013.
21. H. I. Karunadasa, E. Montalvo, Y. Sun, M. Majda, J. R. Long, and C. J. Chang, *Science*, 2012, **335**, 698–702.
22. D. Kong, H. Wang, J. J. Cha, M. Pasta, K. J. Koski, J. Yao, and Y. Cui, *Nano Lett.*, 2013, **13**, 1341–1347.
23. S. Helveg, J. Lauritsen, E. Lægsgaard, I. Stensgaard, J. K. Nørskov, B. S. Clausen, H. Topsøe, and F. Besenbacher, *Phys. Rev. Lett.*, 2000, **84**, 951–954.
24. M. V. Bollinger, J. V. Lauritsen, K. W. Jacobsen, J. K. Nørskov, S. Helveg, and F. Besenbacher, *Phys. Rev. Lett.*, 2001, **87**, 196803.
25. M. V. Bollinger, K. W. Jacobsen, and J. K. Nørskov, *Phys. Rev. B*, 2003, **67**, 085410.
26. J. V. Lauritsen, M. V. Bollinger, E. Lægsgaard, K. W. Jacobsen, J. K. Nørskov, B. S. Clausen, H. Topsøe, and F. Besenbacher, *J. Catal.*, 2004, **221**, 510–522.
27. H. Wang, D. Kong, P. Johanes, J. J. Cha, G. Zheng, K. Yan, N. Liu, and Y. Cui, *Nano Lett.*, 2013, 3426–3433.
28. H. Tang, K. Dou, C. C. Kaun, and Q. Kuang, *J. Mater. Chem. A*, 2014, **2**, 360–364.
29. Q. Yan, C. Xu, P. Shengjie, C. Tan, and H. Tan, *J. Mater. Chem. A*, 2014, **2**, 5597–5601.
30. P. Giannozzi, S. Baroni, N. Bonini, M. Calandra, R. Car, C. Cavazzoni, D. Ceresoli, G. L. Chiarotti, M. Cococcioni, I. Dabo, A. Dal Corso, S. de Gironcoli, S. Fabris, G. Fratesi, R. Gebauer, U. Gerstmann, C. Gougoussis, A. Kokalj, M. Lazzeri, L. Martin-Samos, N. Marzari, F. Mauri, R. Mazzarello, S. Paolini, A. Pasquarello, L. Paulatto, C. Sbraccia, S. Scandolo, G. Sclauzero, A. P. Seitsonen, A. Smogunov, P. Umari, and R. M. Wentzcovitch, *J. Phys.: Condens. Matter*, 2009, **21**, 395502.
31. J. Wellendorff, K. T. Lundgaard, A. Møgelhøj, V. Petzold, D. D. Landis, J. K. Nørskov, T. Bligaard, and K. W. Jacobsen, *Phys. Rev. B*, 2012, **85**, 235149.
32. M. Dion, H. Rydberg, E. Schröder, D. C. Langreth, and B. I. Lundqvist, *Phys. Rev. Lett.*, 2004, **92**, 246401.
33. T. Thonhauser, V. R. Cooper, S. Li, A. Puzder, P. Hyldgaard, and D. C. Langreth, *Phys. Rev. B*, 2007, **76**, 125112.
34. G. Román-Pérez and J. M. Soler, *Phys. Rev. Lett.*, 2009, **103**, 096102.
35. L. H. Brixner, *J. Inorg. Nucl. Chem.*, 1962, **24**, 257–263.
36. B. Hinnemann, J. K. Nørskov, and H. Topsøe, *J. Phys. Chem. B*, 2005, **109**, 2245–2253.
37. H. J. Monkhorst and J. D. Pack, *Phys. Rev. B*, 1976, **13**, 5188–5192.
38. P. Raybaud, J. Hafner, G. Kresse, S. Kasztelan, and H. Toulhoat, *J. Catal.*, 2000, **190**, 128–143.
39. A. A. Peterson, F. Abild-Pedersen, F. Studt, J. Rossmeisl, and J. K. Nørskov, *Energy Environ. Sci.*, 2010, **3**, 1311.
40. M. Pourbaix, *Atlas D'equilibres Electrochimiques*, Gauthier-Villars, Paris, 1963.
41. B. Hammer, L. B. Hansen, and J. K. Nørskov, *Phys. Rev. B*, 1999, **59**, 7413.
42. F. Jellinek, G. Brauer, and H. Müller, *Nature*, 1960, **185**, 376–377.
43. J. C. Wildervanck and F. Jellinek, *Z. Anorg. Allg. Chem.*, 1964, **328**, 309–318.
44. C. Tsai, F. Abild-Pedersen, and J. K. Nørskov, *Nano Lett.*, 2014, **14**, 1381–1387.
45. E. Skúlason, V. Tripkovic, M. E. Björketun, S. Gudmundsdóttir, G. S. Karlberg, J. Rossmeisl, T. Bligaard, H. Jónsson, and J. K. Nørskov, *J. Phys. Chem. C*, 2010, **114**, 18182–18197.
46. B. Hammer and J. K. Nørskov, *Surf. Sci.*, 1995, **343**, 211–220.
47. B. Hammer and J. K. Nørskov, *Adv. Catal.*, 2000, **45**, 71–129.
48. A. Vojvodic, J. K. Nørskov, and F. Abild-Pedersen, *Top. Catal.*, 2013, **57**, 25–32.